

# A possible connection between the spin temperature of damped Lyman- $\alpha$ absorption systems and star formation history

S. J. Curran<sup>\*</sup>

*School of Chemical and Physical Sciences, Victoria University of Wellington, PO Box 600, Wellington 6140, New Zealand*

Accepted —. Received —; in original form —

## ABSTRACT

We present a comprehensive analysis of the spin temperature/covering factor degeneracy,  $T_{\text{spin}}/f$ , in damped Lyman- $\alpha$  absorption systems. By normalising the upper limits and including these via a survival analysis, there is, as previously claimed, an apparent increase in  $T_{\text{spin}}/f$  with redshift at  $z_{\text{abs}} \gtrsim 1$ . However, when we account for the geometry effects of an expanding Universe, neglected by the previous studies, this increase in  $T_{\text{spin}}$  at  $z_{\text{abs}} \gtrsim 1$  is preceded by a decrease at  $z_{\text{abs}} \lesssim 1$ . Using high resolution radio images of the background continuum sources, we can transform the  $T_{\text{spin}}/f$  degeneracy to  $T_{\text{spin}}/d_{\text{abs}}^2$ , where  $d_{\text{abs}}$  is the projected linear size of the absorber. Again, there is no overall increase with redshift, although a dip at  $z_{\text{abs}} \approx 2$  persists. Furthermore, we find  $d_{\text{abs}}^2/T_{\text{spin}}$  to follow a similar variation with redshift as the star formation rate,  $\psi_*$ . This suggests that, although the total hydrogen column density,  $N_{\text{HI}}$ , shows little relation to  $\psi_*$ , the fraction of the cold neutral medium,  $\int \tau_{\text{obs}} dv/N_{\text{HI}}$ , may. Therefore, further efforts to link the neutral gas with the star formation history should also consider the cool component of the gas.

**Key words:** galaxies: high redshift – galaxies: star formation – galaxies: evolution – galaxies: ISM – quasars: absorption lines – radio lines: galaxies

## 1 INTRODUCTION

Studies of redshifted absorption systems lying along the sight-lines to distant quasi-stellar objects (QSOs) provide a probe of the evolution of quiescent galaxies over the history of the Universe. Of particular interest are the so called damped Lyman- $\alpha$  absorption systems (DLAs), since their high defining neutral hydrogen (H I) column densities of  $N_{\text{HI}} \geq 2 \times 10^{20} \text{ cm}^{-2}$  act as signatures for distant gas rich galaxies<sup>1</sup>, fuelling the possible star formation (Neeleman et al. 2017).<sup>2</sup> The Lyman- $\alpha$  transition occurs in the ultra-violet band at  $\lambda_{\text{rest}} = 1216 \text{ \AA}$ , and so is only redshifted into the atmospheric observing window at  $z \gtrsim 1.7$ . In addition to space-based observations of this transition, neutral hydrogen can be detected from  $z \geq 0$  via the  $\lambda_{\text{rest}} = 21.1\text{-cm}$  spin-flip transition. The combination of H I 21-cm and Lyman- $\alpha$  data can yield important information about the high redshift Universe, such as testing for any evolution in the fundamental constants (see Curran et al. 2004a; Ztanavaris et al. 2005) and measuring the temperature, and

thus star-forming potential, of the neutral gas in the most distant galaxies (e.g. Wolfe et al. 2003).

The spin temperature,  $T_{\text{spin}}$ , of the gas is a measure of the population of the lower hyperfine level ( $F = 1$ ), where the gas can absorb 21-cm photons, relative to the upper hyperfine level ( $F = 2$ ). Thus, the spin temperature can be raised via excitation to the upper hyperfine level by 21-cm absorption (Purcell & Field 1956), excitation above ground state by Lyman- $\alpha$  absorption (Field 1959) and collisional excitation (Bahcall & Ekers 1969). Presuming that the Lyman- $\alpha$  and 21-cm absorption trace the same sight-line, the spin temperature can be obtained by comparing the velocity integrated optical depth of the 21-cm absorption strength,  $\int \tau dv$ , with the total neutral hydrogen column density, via (e.g. Rohlfs & Wilson 2000)

$$N_{\text{HI}} = 1.823 \times 10^{18} T_{\text{spin}} \int \tau dv. \quad (1)$$

The observed optical depth is the ratio of the line depth,  $\Delta S$ , to the observed background flux,  $S_{\text{obs}}$ , and is related to the intrinsic optical depth via

$$\tau \equiv -\ln \left( 1 - \frac{\tau_{\text{obs}}}{f} \right) \approx \frac{\tau_{\text{obs}}}{f}, \text{ for } \tau_{\text{obs}} \equiv \frac{\Delta S}{S_{\text{obs}}} \lesssim 0.3, \quad (2)$$

where the covering factor,  $f$ , is the fraction of  $S_{\text{obs}}$  intercepted by the absorber. Therefore, in the optically thin regime (where  $\tau_{\text{obs}} \lesssim$

<sup>\*</sup> Stephen.Curran@vuw.ac.nz

<sup>1</sup> DLAs may account for at least 80% of the neutral gas mass density in the Universe (Prochaska et al. 2005).

<sup>2</sup> From two  $z \sim 4$  DLAs recently detected in [C II] 158  $\mu\text{m}$  emission. This arises from heated dust, generally believed to be caused by a stellar population (e.g. Maiolino et al. 2005), although heating by an active nucleus is also a possibility (Curran 2009).

0.3), Equ. 1 can be rewritten as

$$N_{\text{HI}} \approx 1.823 \times 10^{18} \frac{T_{\text{spin}}}{f} \int \tau_{\text{obs}} dv, \quad (3)$$

so that the comparison of the neutral hydrogen column density with the observed velocity integrated optical depth of the 21-cm absorption gives the degenerate  $T_{\text{spin}}/f$ . Since, by definition,  $\tau_{\text{obs}} < f \leq 1$  (the lower limit being imposed by Equ. 2, O’Dea et al. 1994), then  $\tau_{\text{obs}} \leq \tau$  and if  $\tau_{\text{obs}} < \tau$ , the observed absorption strength is diluted. That is, assuming  $f = 1$ , when in reality  $f < 1$ , has the effect of artificially raising the apparent spin temperature (see figure 1 of Curran et al. 2005).

Since Kanekar & Chengalur (2003) noted a mix of 21-cm detections and non-detections in DLAs at  $z_{\text{abs}} \lesssim 2$ , whereas at  $z_{\text{abs}} \gtrsim 2$  detections were rare, they suggested that the lower redshift DLAs had a mix of spin temperatures with the higher redshift DLAs having exclusively high spin temperatures, suggesting an “evolution” in the temperature of the gas. However, Curran et al. (2005) argued that, since  $T_{\text{spin}}/f$  was degenerate, the values of  $T_{\text{spin}}$  obtained by Kanekar & Chengalur (2003) could be due to their estimates of  $f = 1$  for all of the highest redshift absorbers. Following this, Curran & Webb (2006) showed that, due to the geometry of an expanding Universe, low redshift absorbers could be at lower angular diameter distances than the background QSOs, whereas at higher redshift the angular diameter distance to the absorber is always similar to that to the QSO ( $DA_{\text{DLA}} \approx DA_{\text{QSO}}, \forall z_{\text{abs}} \gtrsim 1.6$ ), no matter the relative redshifts (see Sect. 2.2). Since, to a first order, the covering factor is proportional to the ratio of the angular diameter distances, Curran & Webb argued that this distribution could in fact be the cause of the observed  $T_{\text{spin}}/f$ –redshift distribution, with Curran (2012) showing that the factor of two between the mean values of  $T_{\text{spin}}/f$  (1800 K at  $z_{\text{abs}} < 2$  and 3600 K at  $z_{\text{abs}} > 2$ ) could be accounted by the difference in angular diameter distance ratios between these two redshift ranges. Thus, the observed  $T_{\text{spin}}/f$ –redshift distribution could be explained by the geometry effects of an expanding Universe, not requiring an evolution in the spin temperature.

Since then, several studies have reasserted that the spin temperature increases with redshift, although these avoid the geometry effects by only considering a limited redshift range ( $z_{\text{abs}} > 2$  by Roy et al. 2013 and  $z_{\text{abs}} > 1$  by Kanekar et al. 2014). This excludes over half of the Universe (as well as 30% of the sample, Fig. 1), and obviously cannot test the original hypothesis of Kanekar & Chengalur (2003) that there is a difference in the spin temperatures between the low and high redshift samples. In this paper we undertake a full analysis by incorporating the geometry effects in order to determine whether there is an evolution in the spin temperature over the full  $\approx 12$  Gyr probed.

## 2 ANALYSIS

### 2.1 Normalisation and inclusion of the limits

In order to normalise the search sensitivities, which are quoted over a large range of spectral resolutions (Fig. 2)<sup>3</sup>, and thus meaningless

<sup>3</sup> The 21-cm searches are compiled from Davis & May (1978); Brown & Spencer (1979); Briggs & Wolfe (1983); Chengalur & Kanekar (2000); Kanekar et al. (2001a,b, 2009b, 2013, 2014); Briggs et al. (2001); Kanekar & Chengalur (2001, 2003); Curran et al. (2005, 2007, 2010); York et al. (2007); Gupta et al. (2009a,b); Ellison et al. (2012); Srianand et al. (2012); Roy et al. (2013); Kanekar (2014).

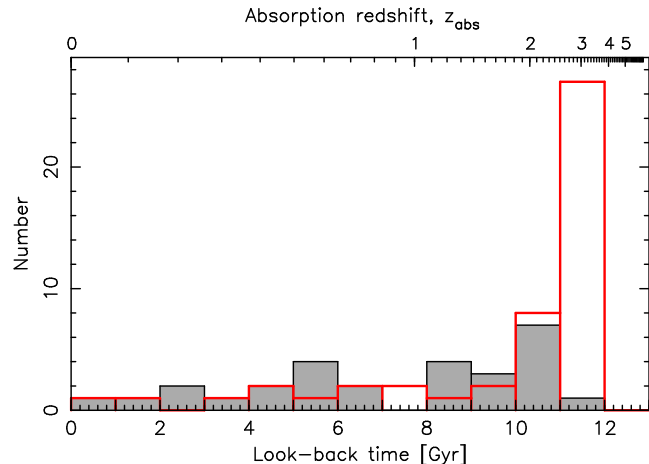


**Figure 1.** The distribution of the 21-cm detections (shaded histogram) and non-detections (unshaded) with look-back time. Throughout the paper we use a standard  $\Lambda$  cosmology with  $H_0 = 71 \text{ km s}^{-1} \text{ Mpc}^{-1}$ ,  $\Omega_{\text{matter}} = 0.27$  and  $\Omega_{\Lambda} = 0.73$ .

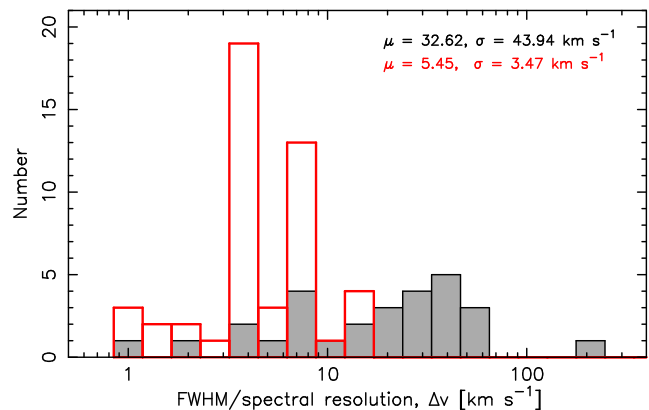


**Figure 2.** The distribution of spectral resolution (for the non-detection, unshaded) and the line-widths (for the detections, shaded). The non-detections span a range of  $0.93 - 15 \text{ km s}^{-1}$ , which are too disparate to show clearly on a linear scale.

to compare directly, we have to re-sample the r.m.s. noise levels to a common channel width. We then use this as the full-width half maximum (FWHM) of the putative absorption profile, thus giving a normalised velocity integrated optical depth per channel limit to all of the non-detections (see Curran 2012 for details). We use the mean  $\langle \text{FWHM} \rangle = 33 \text{ km s}^{-1}$  for the detections to recalculate the limit to  $T_{\text{spin}}/f$  for each non-detection. Note that there is no significant difference between the FWHMs of the low and high redshift intervening 21-cm absorbers (Curran et al. 2016a), and so we do not apply any redshift dependence.

In order to fully utilise these data, we include the lower limits to  $T_{\text{spin}}/f$  (from the non-detections) via the *Astronomy SURVival Analysis* (ASURV) package (Isobe et al. 1986), which are added to the analysis as censored data points (Fig. 3, top). For the bivariate data, a generalised non-parametric Kendall-tau test gives a probability of  $P(\tau) = 3.60 \times 10^{-3}$  of the observed  $T_{\text{spin}}/f$ – $z_{\text{abs}}$  correlation arising by chance, which is significant at  $S(\tau) = 2.91\sigma$ , assuming Gaussian statistics. For the binned data, the limits are incorporated, via the Kaplan–Meier estimator, which gives a maximum-likelihood estimate based upon the parent population (Feigelson & Nelson 1985). As a visual representation to comple-

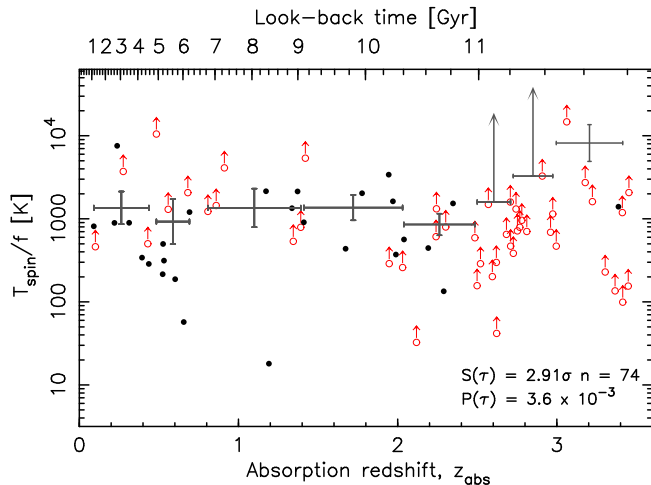


**Figure 3.** The spin temperature/covering factor ratio versus the redshift for the DLAs searched in 21-cm absorption. The filled circles show the detections, the unfilled circles the lower limits and the error bars the binned values including the limits. The horizontal bars show the range of points in the bin and the vertical error bars the  $1\sigma$  uncertainty in the mean value.

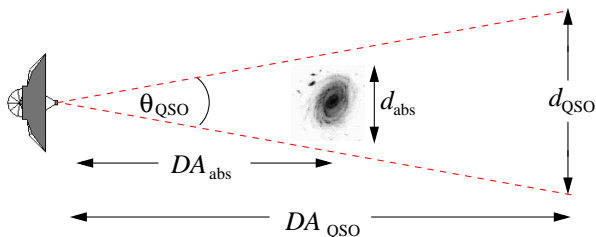


**Figure 4.** The projected absorber ( $d_{\text{abs}}$ ) and emitter cross-sections ( $d_{\text{QSO}}$ ) with respect to their angular diameter distances ( $DA_{\text{abs}}$  and  $DA_{\text{QSO}}$ ).  $\theta_{\text{QSO}}$  is the angle subtended by the background emission. For a disk inclination of  $i$  (where  $i = 90^\circ$  for face-on)  $d_{\text{abs}} = d_{\text{HI}} \sin i$ , where  $d_{\text{HI}}$  is the actual diameter of the HI disk. For intervening absorption we expect a close to face-on inclination (e.g. Curran et al. 2016b). Adapted from Curran (2012).

ment the Kendall-tau test, it is apparent that  $T_{\text{spin}}/f$  does exhibit an increase with redshift.

## 2.2 Correcting for geometry

The positive  $T_{\text{spin}}/f$ - $z_{\text{abs}}$  correlation could support the recent studies which conclude that there is an increase in the spin temperature with redshift. However, as stated in Sect. 1, none of these account for the geometry effects of an expanding Universe, thus neglecting half of its history, which must be accounted for prior to invoking any cosmic evolution. In the small angle approximation, the covering factor is given by (Curran 2012; Allison et al. 2016, see Fig. 4).

$$f = \begin{cases} \frac{d_{\text{abs}}^2}{DA_{\text{abs}}^2 \theta_{\text{QSO}}^2} & \text{if } \theta_{\text{abs}} < \theta_{\text{QSO}} \\ 1 & \text{if } \theta_{\text{abs}} \geq \theta_{\text{QSO}}, \end{cases} \quad (4)$$

where the angular diameter distance to a source is given by

$$DA = \frac{DC}{z+1}, \quad \text{where } DC = \frac{c}{H_0} \int_0^z \frac{dz}{H_z/H_0} \quad (5)$$

is the line-of-sight co-moving distance (e.g. Peacock 1999), in which  $c$  is the speed of light,  $H_0$  the Hubble constant,  $H_z$  the Hub-

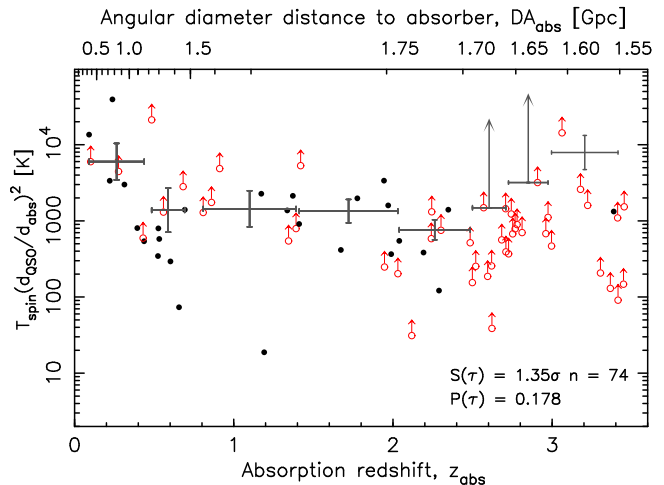


**Figure 5.** The  $T_{\text{spin}}/f$ - $z$  distribution (Fig. 3) corrected for the angular diameter distances.

ble parameter at redshift  $z$  and

$$\frac{H_z}{H_0} = \sqrt{\Omega_m (z+1)^3 + (1 - \Omega_m - \Omega_\Lambda) (z+1)^2 + \Omega_\Lambda}. \quad (6)$$

For a standard  $\Lambda$  cosmology, this gives a peak in the angular diameter distance at  $z \approx 1.6$ , meaning that objects beyond this redshift are all essentially at the same angular diameter distance of  $DA \approx 1500 - 1700$  Mpc, irrespective of their co-moving distances.<sup>4</sup> This has the consequence that at low redshift it is possible for  $DA_{\text{abs}} < DA_{\text{QSO}}$  (when  $z_{\text{abs}} < z_{\text{QSO}}$ ), giving the familiar angular size–distance relation. However, at high redshift only  $DA_{\text{abs}} \approx DA_{\text{QSO}}$  is possible, which will introduce a bias to the covering factor between the low and high redshift regimes. Therefore, in Fig. 5 we correct for the angular diameter distances by scaling  $T_{\text{spin}}/f$  by  $\left(\frac{DA_{\text{QSO}}}{DA_{\text{abs}}}\right)^2$ , giving  $T_{\text{spin}} \left(\frac{d_{\text{QSO}}}{d_{\text{abs}}}\right)^2$  on the ordinate. This causes the correlation evident in Fig. 3 to disappear, although there will appear to be a strong increase in  $T_{\text{spin}}/f$  with redshift if the  $z_{\text{abs}} \lesssim 1$  data are ignored (Roy et al. 2013; Kanekar et al. 2014).

## 2.3 Normalisation by emitter extent

The correction for the geometry effects indicates a decrease in  $T_{\text{spin}}/f$  with redshift over the most recent half of the Universe's history, followed by an increase over the first half. Whether this is dominated by the spin temperature or the covering factor remains unknown, although we can attempt to break the degeneracy by deconstructing the covering factor. Previous studies attempt to estimate the covering factor by assuming that this is given by the ratio of the flux from the compact unresolved component of the radio emission to the total radio continuum flux (e.g. Briggs & Wolfe 1983; Kanekar et al. 2009a, 2013, 2014). However, the ratio of the fluxes contains no information on the depth of the line when the extended continuum emission is resolved out, the extent of the absorber, nor how this is aligned along the sight-line to the QSO.

Referring to Equ. 4, however, we do know the angular diameter distances and in many cases the extent of the emission is known from high resolution radio imaging (Kanekar et al. 2009a, 2013, 2014; Ellison et al. 2012), which are resolved at  $\theta_{\text{QSO}} = 1.6 - 82$

<sup>4</sup> See the top scale of Fig. 5.

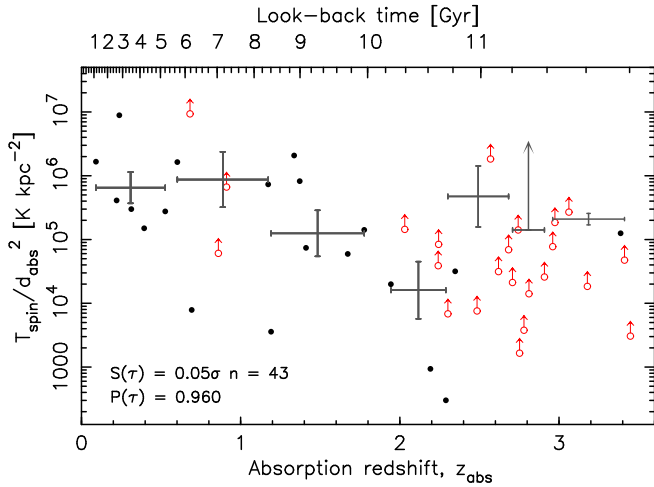


**Figure 6.** The spin temperature degenerate/absorber size versus the redshift.

mas. So in addition to removing the angular diameter distances (Sect. 2.2), we can remove  $d_{\text{QSO}} = \theta_{\text{QSO}} D A_{\text{QSO}}$ , giving

$$\frac{T_{\text{spin}}}{d_{\text{abs}}^2} = \frac{N_{\text{HI}}}{1.823 \times 10^{18} (\theta_{\text{QSO}} D A_{\text{abs}})^2 \int \tau_{\text{obs}} dv}, \quad (7)$$

where  $\theta_{\text{QSO}} D A_{\text{abs}}$  is the linear size of the QSO at  $z_{\text{abs}}$ . Showing this in Fig. 6, we see that any hint of a correlation disappears, although a dip at  $z_{\text{abs}} \sim 2$  persists. The dip has a value of  $\log_{10}(T_{\text{spin}}/d_{\text{abs}}^2) = 4.21 \pm 0.45$  at  $z_{\text{abs}} = 2.12 \pm 0.71$  and comparing this with the neighbouring bins,

- $z_{\text{abs}} = 1.48 \pm 0.29$  is offset by  $1.99\sigma$  in  $\log_{10}(T_{\text{spin}}/d_{\text{abs}}^2)$ , although this bin may be part of the dip, so
- $z_{\text{abs}} = 0.89 \pm 0.29$  is offset by  $3.87\sigma$ ,
- $z_{\text{abs}} = 2.49 \pm 0.19$  is offset by  $3.67\sigma$ .

Therefore the dip is significant. The bin size is chosen to minimise the remaining unbinned data, while being sufficiently coarse to display any trends in the data. For example, there are 43 data points in Fig. 6, which are binned into groups of six leaving one unbinned point (at the highest  $z_{\text{abs}}$ ). If we rebin the data, in three bins of 14 (again with a remainder of one), for

- $z_{\text{abs}} = 0.71 \pm 0.62$ ,  $\log_{10}(T_{\text{spin}}/d_{\text{abs}}^2) = 5.73 \pm 0.27$ ,
- $z_{\text{abs}} = 1.97 \pm 0.60$ ,  $\log_{10}(T_{\text{spin}}/d_{\text{abs}}^2) = 4.96 \pm 0.32$ ,
- $z_{\text{abs}} = 3.02 \pm 0.40$ ,  $\log_{10}(T_{\text{spin}}/d_{\text{abs}}^2) = 5.35 \pm 0.07$ ,

and so the dip persists in the middle bin (see Fig. 10). The first bin is offset by  $2.40\sigma$  from this, but the last is only  $1.22\sigma$ , although this may be related to the star formation history (see Sect. 3).

## 2.4 Metallicity

Since the heavy element abundance is expected to decrease with look-back time (e.g. Prochaska et al. 2003; Curran et al. 2004b; Rafelski et al. 2012), in addition to the metals providing radiation pathways for the gas to cool (e.g. Wolfire et al. 1995), it has been argued that the anti-correlation between the (estimated) spin temperature and metallicity,  $[M/H]$ , is evidence for an evolution in  $T_{\text{spin}}$  with redshift (Kanekar et al. 2009c). However, of the 13 low redshift ( $z_{\text{abs}} \lesssim 1$ ) DLAs which have measured metallicities (Fig. 7), only three are non-detected in 21-cm absorption, which does not support the hypothesis of Kanekar & Chengalur (2003) that a mix of spin temperatures should give a mix of metallicities.

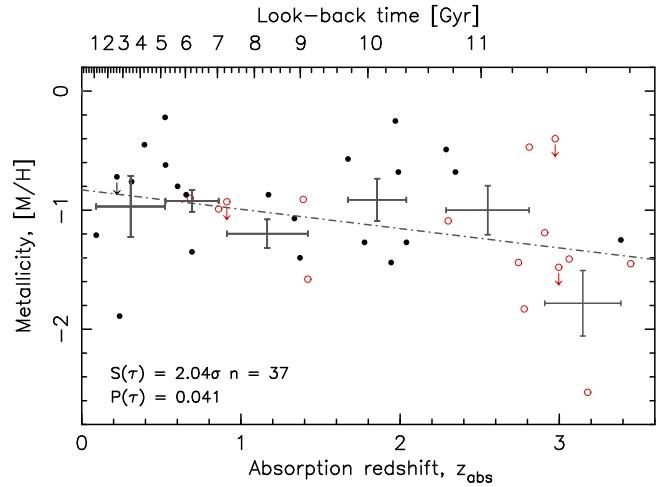


**Figure 7.** The metallicity versus redshift for the 21-cm absorption searches, where available. The line shows the least-squares fit to the data.

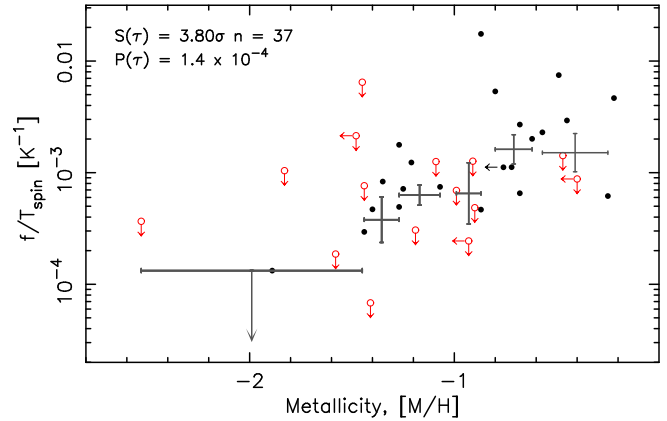


**Figure 8.**  $f/T_{\text{spin}}$  versus the metallicity. We invert the ordinate from  $T_{\text{spin}}/f$  since ASURV cannot mix upper and lower limits.

Curran et al. (2007) suggested that the anti-correlation between  $T_{\text{spin}}/f$  and  $[M/H]$  could be driven by the covering factor: A correlation between metallicity and velocity spread in low ionisation species had been noted (Ledoux et al. 2006; Murphy et al. 2007). If attributed to galactic dynamics (Wolfe & Prochaska 1998; Khare et al. 2007; Prochaska et al. 2008), this spread indicates that metallicity is a tracer of mass, perhaps supporting the argument that the covering factor, through galaxy size, is dominant in the correlation.

We update the plot of  $T_{\text{spin}}/f$  versus  $z_{\text{abs}}$  in Fig. 8, where we see the correlation strengthens over the previous values of  $2.80\sigma$  (Curran et al. 2007) and  $3.07\sigma$  (Curran et al. 2010). Again, however, it is difficult to break the  $T_{\text{spin}}/f$  degeneracy, although we can apply the above methods to yield  $d_{\text{abs}}^2/T_{\text{spin}}$  (Fig. 9). This weakens the correlation, although the nine missing data points, due to not having a measurement of  $\theta_{\text{QSO}}$ , are mostly detected points (which are used to determine the censored values) from one end of the distribution (top right). So a weakening of the correlation is not unexpected and it remains plausible that  $d_{\text{abs}} \propto [M/H]$ .

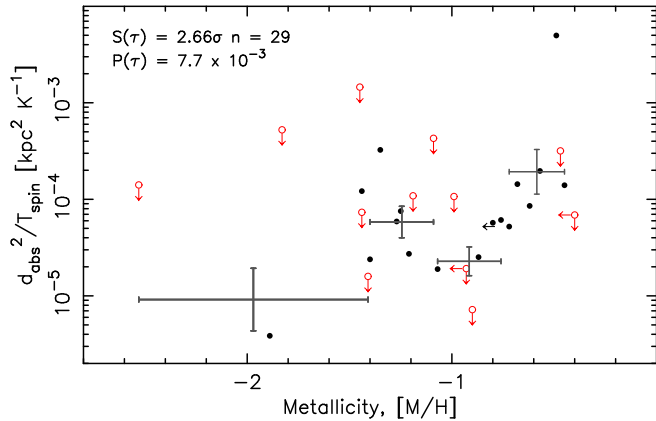


**Figure 9.** As Fig. 8, but with the removal of the angular diameter distances and  $d_{\text{QSO}}$  (cf. Equ. 7).

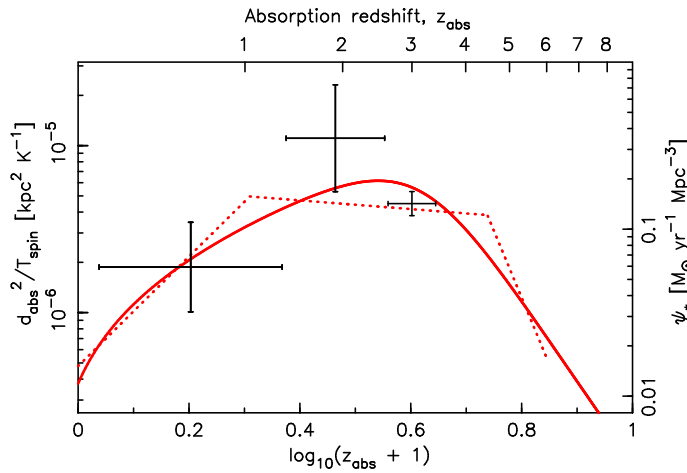


**Figure 10.** The error bars in Fig. 6 with the ordinate re-binned and inverted and the abscissa mapped to  $\log_{10}(z_{\text{abs}} + 1)$ , in order to overlay the best fit curve to the SFR density—redshift distribution from Hopkins & Beacom (2006) [the dotted lines show the piecewise linear fitting results]. These have been arbitrarily shifted on the ordinate but retain the relative scaling (right hand scale).

### 3 STAR FORMATION HISTORY

Although we find no clear evolution in the spin temperature degenerate with absorber size, the binned values of  $T_{\text{spin}}/d_{\text{abs}}^2$  are indicative of a dip at  $z_{\text{abs}} \approx 2$  (Fig. 6). This is close to where the star formation rate density,  $\psi_*$ , peaks (Hopkins & Beacom 2006; Burgarella et al. 2013; Sobral et al. 2013; Lagos et al. 2014; Madau & Dickinson 2014; Zwart et al. 2014). In contrast, the mass density of neutral hydrogen rises from  $\Omega_{\text{HI}} \approx 0.5 \times 10^{-3}$  at  $z \lesssim 0.5$  (Zwaan et al. 2005; Lah et al. 2007; Braun 2012; Delhaize et al. 2013; Rhee et al. 2013; Hoppmann et al. 2015; Neeleman et al. 2016), but remains flat at  $\Omega_{\text{HI}} \approx 1 \times 10^{-3}$  over  $0.5 \gtrsim z \gtrsim 5$  (Rao & Turnshek 2000; Prochaska & Herbert-Fort 2004; Rao et al. 2006; Curran 2010; Prochaska & Wolfe 2009; Noterdaeme et al. 2012; Crighton et al. 2015). This has led to a much debated disparity between the fuel for star formation and the star formation history.

From the binned values of  $d_{\text{abs}}^2/T_{\text{spin}}$ , however, we find a reasonable, albeit coarse, trace of the star formation history (Fig. 10). Given that star formation occurs in cold ( $\sim 10$  K), dense ( $\sim 10^3$  atoms  $\text{cm}^{-3}$ ) gas, this could indicate that the fraction of the cold

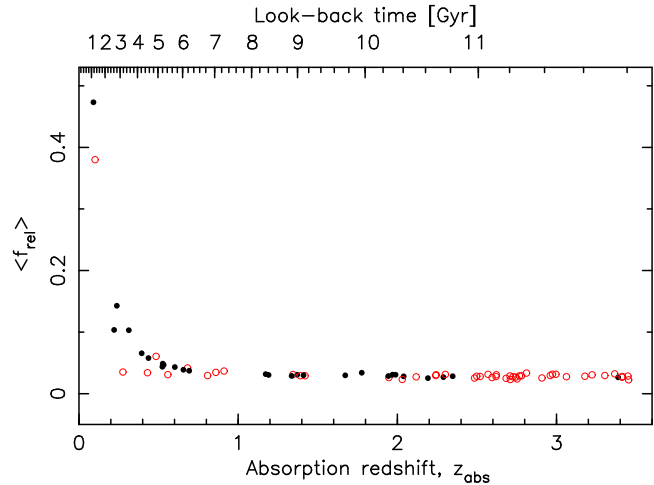


**Figure 11.** The expectation value of the relative covering factor.

neutral medium (CNM, where  $T \sim 150$  K and  $n \sim 10 \text{ cm}^{-3}$ ) is a more suitable tracer of the reservoir for star formation than the bulk of the neutral gas, which also consists of the warm neutral medium (WNM, where  $T \sim 8000$  K and  $n \sim 0.2 \text{ cm}^{-3}$ , Wolfire et al. 1995). By definition, the CNM fraction is ratio of cold to total neutral gas, i.e.  $\propto \int \tau_{\text{obs}} dv / N_{\text{HI}}$ , which we see to peak at a similar redshift as  $\psi_*$ , when the geometry effects have been accounted for (Figs. 5 & 6).

## 4 CAVEATS

### 4.1 Absorber–QSO alignment

From Fig. 4 it is clear that Equ. 4 only holds for direct alignment between the absorber and the QSO, although, for a given  $d_{\text{abs}}$  and  $d_{\text{QSO}}$ , interception of the QSO is more likely when  $z_{\text{abs}} \ll z_{\text{QSO}}$ . For a given sight-line, if there is no information on the impact parameter, the covering factor will vary randomly over  $f = 0 - 1$ . We therefore run a Monte-Carlo simulation with 10 000 iterations, where the probability of interception is a random value between 0 and 1 scaled by the angular diameter ratio,  $(DA_{\text{QSO}}/DA_{\text{abs}})^2$ , to yield the expectation value of the covering factor (Fig. 11). Since we do not know the absolute covering factor, this is scaled according to the maximum measured ratio, i.e.  $DA_{\text{QSO}}/DA_{\text{abs}} = 4.09$ , giving  $\langle f_{\text{rel}} \rangle \approx 0.5$  for the lowest redshift point, where the ratio is normalised out. The distribution essentially traces the angular diameter distance ratios of the sample (Curran 2012), but halved and inverted. It should be noted that this is just a statistical relative expectation value for the covering factor. It is, however, consistent with the simulations of Kanekar et al. (2014) which find that the covering factors do not vary significantly at  $z_{\text{abs}} > 1$  (cf. Fig. 11).

### 4.2 Absorber sizes

Again, referring to Equ. 4, the above analysis only holds for  $\theta_{\text{abs}} < \theta_{\text{QSO}}$ , i.e.  $d_{\text{abs}} < DA_{\text{abs}}\theta_{\text{QSO}}$ , otherwise  $f = 1$  and the spin temperature can be determined. In Fig. 12 we show the distribution of  $DA_{\text{abs}}\theta_{\text{QSO}}$  with  $z_{\text{abs}}$  for which we see that the lowest redshift absorbers need a projected extent exceeding  $d_{\text{abs}} \sim 50$  pc to have  $f \approx 0.5$ , taking into account the alignment (Sect. 4.1), requiring  $d_{\text{HI}} \gtrsim 0.1$  kpc for  $f \approx 1$  (Fig. 4). However, without knowing the

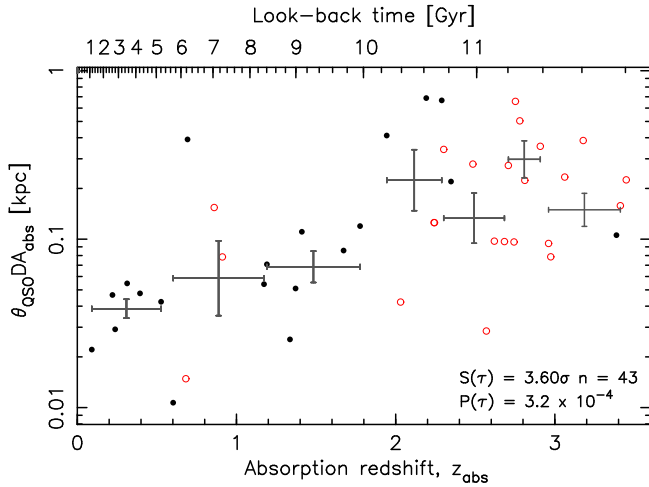


**Figure 12.** The linear extent of the QSO at the absorption redshift versus the absorption redshift.

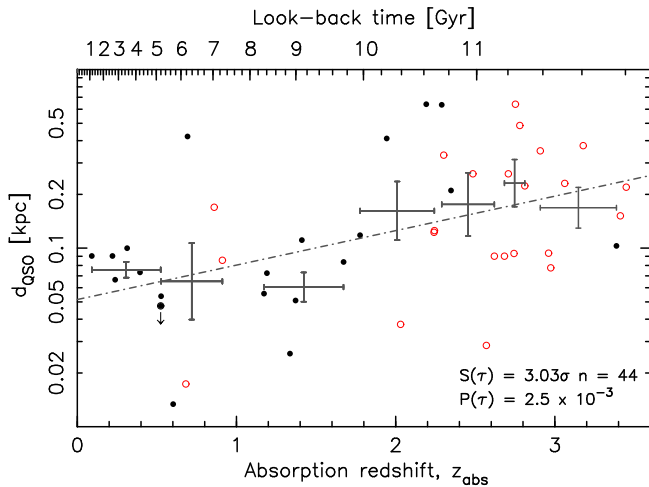


**Figure 13.** The linear extent of the QSO versus the absorption redshift. The line shows the least-squares fit to the data. A similar correlation between  $d_{\text{QSO}}$  and  $z_{\text{abs}}$  was noted for the 25 measurements then available by Kanekar et al. (2009a).

projected size,  $d_{\text{abs}}$ , we cannot say which of the sample are sufficiently large to have a covering factor of unity, although the deprojected sizes are suspected to be  $d_{\text{HI}} \sim 0.1 - 1$  kpc in the case of near-by associated absorption systems (Braun 2012; Curran et al. 2013). If, for the sake of argument, we say that  $f \approx 1$  for the cases where  $DA_{\text{abs}}\theta_{\text{QSO}} \lesssim 0.1$  kpc, this would imply that  $f \sim 1$  at  $z_{\text{abs}} \lesssim 2$ , at least where the source sizes have been measured. This, in conjunction with the flattening of the angular diameter distance above these redshifts (Sect. 2.2), may indicate that no correction for geometry is required. However, it is clear from Fig. 12 that the high redshift absorbers need to be significantly larger than their low redshift counterparts in order that  $f = 1$  and therefore  $f$  is likely to decrease with redshift. This increase in QSO size is most likely due to the Malmquist bias favouring the largest and brightest radio sources at high redshift (Fig. 13).

It is, of course, possible that the increase in radio source size with redshift is matched with an increase in absorber size, but given that there is a well documented evolution in galaxy sizes, where large galaxies dominate the low redshift population

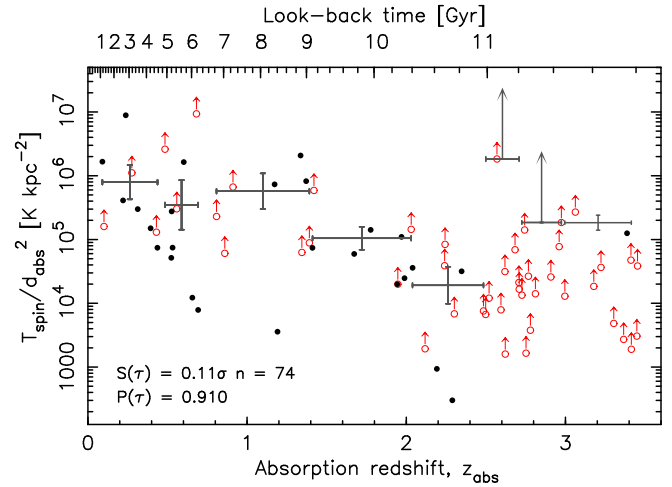


**Figure 14.** As Fig. 6, but with the unmeasured values of  $d_{\text{QSO}}$  estimated from the fit in Fig. 13.

(Baker et al. 2000) and dwarf galaxies the high redshift population (Lanfranchi & Friaça 2003), this is unlikely.

On this matter, it is possible that the decrease in  $d_{\text{abs}}^2/T_{\text{spin}}$  at high redshift (Fig. 10) is due to galaxy size evolution. For massive ( $\geq 10^{11} M_{\odot}$ ) galaxies, which are the easiest to resolve at high redshift, the average galaxy size decreases by a factor of  $\approx 3$  over  $0 \lesssim z \lesssim 3$  (Bouwens et al. 2004; Ferguson et al. 2004; Trujillo et al. 2006; Buitrago et al. 2008). If this was applicable to DLAs, it would imply  $d_{\text{abs}}^2(z_{\text{abs}} = 3) \sim 0.1 d_{\text{abs}}^2(z_{\text{abs}} = 0)$ , which could account for the observed  $d_{\text{abs}}^2/T_{\text{spin}}$  distribution, if this ranged from  $z_{\text{abs}} \sim 0$ . However, the decrease in  $d_{\text{abs}}^2/T_{\text{spin}}$  is only observed from  $z_{\text{abs}} \gtrsim 2$  and so the evolution of galaxy sizes cannot account for the increase in  $d_{\text{abs}}^2/T_{\text{spin}}$  at  $z_{\text{abs}} \lesssim 2$ .

### 4.3 QSO structure

Another factor, which is essentially the absorber–QSO alignment (Sect. 4.1) for a non-uniform flux distribution, is that the strength of the absorption will also depend upon any structure in the emission. Here, in the absence of any information regarding the alignment, Equ. 4 assumes uniform flux over the high resolution images (Sect. 2.3), which span  $\lesssim 1$  kpc at the absorption redshift (Sect. 4.2). The specific line-of-sight geometry between the absorber, which may also have structure, and the various components in the emitter, will obviously affect the validity the Eqs. 4 and 7, although not the  $T_{\text{spin}} \left(\frac{d_{\text{QSO}}}{d_{\text{abs}}}\right)^2$  values (Fig. 5), which are only corrected for the angular diameter distances, with the distribution also exhibiting the dip. Although individual values of  $T_{\text{spin}}/d_{\text{abs}}^2$  may not be reliable, statistically we expect these effects to average out, unless there is a further, currently unenvisioned, effect at play.

### 4.4 Limited data

A major caveat of the current analysis is the limited data; only 43 values when we incorporate  $d_{\text{QSO}}$  (Fig. 6). Using the fit in Fig. 13, we can estimate a typical source size from the correlation with redshift, where this has not been measured. Showing this in Figs. 14 and 15, we see that both the  $z_{\text{abs}} \approx 2$  dip and trace of the SFR density persist. However, the fact remains that high resolution radio imaging of the current objects, in addition to 21-cm surveys of

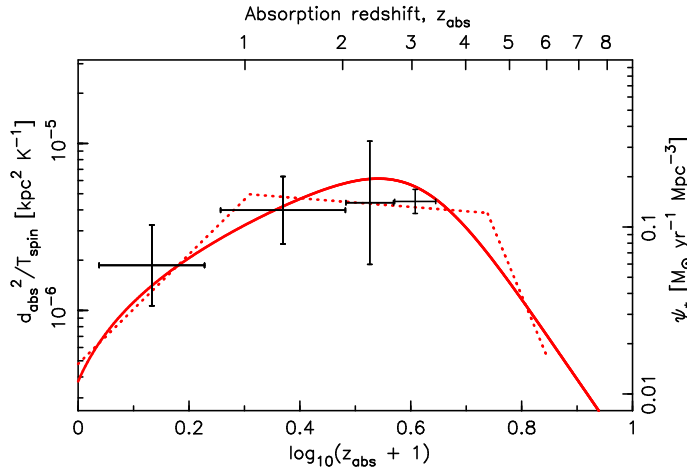


**Figure 15.** As Fig. 10, but with the unmeasured values of  $d_{\text{QSO}}$  estimated from the fit in Fig. 13. The same ordinate shift is used.

$z_{\text{abs}} \gtrsim 4$  DLAs, is required in order to fully investigate any similarity between  $d_{\text{abs}}^2/T_{\text{spin}}$  and the star formation history.

## 5 CONCLUSIONS

We investigate the recent assertions that there is an increase in the spin temperature of damped Lyman- $\alpha$  absorption systems with redshift. In order to address this in a comprehensive and self consistent way, we normalise the limits of the 21-cm absorption searches and include these via a survival analysis, in addition to accounting for the geometry effects of an expanding Universe. These effects are neglected by other studies but are crucial in any complete treatment, since they introduce a systematic difference in the covering factor between the low and high redshift regimes.

Accounting for the geometry effects, we find the correlation of  $T_{\text{spin}}/f$  with redshift to hold only for  $z_{\text{abs}} \gtrsim 1$ , with an anti-correlation below these redshifts. This indicates a minimum in the spin temperature (or a maximum in the covering factor), at  $z_{\text{abs}} \approx 1 - 2$ . Combining the measurements of the background radio sources with the other *known* quantities, the angular diameter distances to the absorber and the QSO, we can obtain  $T_{\text{spin}}/d_{\text{abs}}^2$ , where  $d_{\text{abs}}$  is the projected diameter of the absorber. Using this, thus avoiding the unjustified assumption that the angular size of the absorber is equal to that of the compact flux component, we find a dip to persist, with a minimum  $T_{\text{spin}}/d_{\text{abs}}^2$  at  $z_{\text{abs}} \sim 2$ . Inverting this, giving the fraction of the cold neutral medium, we find  $d_{\text{abs}}^2/T_{\text{spin}} \propto \int \tau_{\text{obs}} dv/N_{\text{HI}}$  to follow the star formation history.

This result does, however, rely upon several assumptions:

(i) That the unknown alignment of the absorber with respect to the sight-line to the QSO, averages out over the sample, making the ratio of angular diameter distances the dominant effect. If this is the case, it should also apply where the flux is not uniform across the radio emission.

(ii) That there is no overwhelming evolution the unknown projected absorber extent,  $d_{\text{abs}}$ , with redshift.

(iii) That  $d_{\text{abs}}$  is smaller than the projected extent of the quasar at the absorption redshift. Even if this is not the case, the covering factor, on the whole, decreases with redshift, requiring a corresponding decrease in spin temperature to produce the observed  $T_{\text{spin}}/f - z_{\text{abs}}$  distribution.

The result also relies upon the coarse binning of the limited data (43 cases where high resolution images are available), to average out these effects. However, if new data confirm this result, it would explain why the evolution of the total neutral hydrogen column density does not trace that of the star formation history and that future efforts should be focused on the cool component of the gas.

## ACKNOWLEDGEMENTS

I wish to thank the referee for their prompt and helpful comments. Also Christian Henkel and James Allison for their very useful feedback, as well as Warren Trotman (RIP) who xfiged the radio telescope in Fig. 4, back in our Masters days at Jodrell bank. I never got to thank him in person. This research has made use of the NASA/IPAC Extragalactic Database (NED) which is operated by the Jet Propulsion Laboratory, California Institute of Technology, under contract with the National Aeronautics and Space Administration and NASA's Astrophysics Data System Bibliographic Service. This research has also made use of NASA's Astrophysics Data System Bibliographic Service and ASURV Rev 1.2 (Lavalley et al. 1992), which implements the methods presented in Isope et al. (1986).

## REFERENCES

- Allison J. R., Zwaan M. A., Duchesne S. W., Curran S. J., 2016, MNRAS, 462, 1341
- Bahcall J. N., Ekers R. D., 1969, ApJ, 157, 1055
- Baker A. C., Mathlin G. P., Churches D. K., Edmunds M. G., 2000, in Star Formation from the Small to the Large Scale, Vol.45 of ESA SP, Favata F., Kaas A., Wilson A., eds., ESA Special Publication, Noordwijk, p. 21
- Bouwens R. J., Illingworth G. D., Blakeslee J. P., Broadhurst T. J., Franx M., 2004, ApJ, 611, L1
- Braun R., 2012, ApJ, 87, 749
- Briggs F. H., de Bruyn A. G., Vermeulen R. C., 2001, A&A, 373, 113
- Briggs F. H., Wolfe A. M., 1983, ApJ, 268, 76
- Brown R. L., Spencer R. E., 1979, ApJ, 230, L1
- Buitrago F., Trujillo I., Conselice C. J., Bouwens R. J., Dickinson M., Yan H., 2008, ApJ, 687, L61
- Burgarella D. et al., 2013, A&A, 554, A70
- Chengalur J. N., Kanekar N., 2000, MNRAS, 318, 303
- Crighton N. H. M. et al., 2015, MNRAS, 452, 217
- Curran S. J., 2009, A&A, 497, 351
- Curran S. J., 2010, MNRAS, 402, 2657
- Curran S. J., 2012, ApJ, 748, L18
- Curran S. J., Allison J. R., Glowacki M., Whiting M. T., Sadler E. M., 2013, MNRAS, 431, 3408
- Curran S. J., Duchesne S. W., Divoli A., Allison J. R., 2016a, MNRAS, 462, 4197
- Curran S. J., Kanekar N., Darling J. K., 2004a, Science with the Square Kilometer Array, New Astronomy Reviews 48, Carilli C. L., Rawlings S., eds., Elsevier, Amsterdam, pp. 1095–1105
- Curran S. J., Murphy M. T., Pihlström Y. M., Webb J. K., Purcell C. R., 2005, MNRAS, 356, 1509
- Curran S. J., Reeves S. N., Allison J. R., Sadler E. M., 2016b, MNRAS, 459, 4136
- Curran S. J., Tzanavaris P., Darling J. K., Whiting M. T., Webb

- J. K., Bignell C., Athreya R., Murphy M. T., 2010, *MNRAS*, 402, 35
- Curran S. J., Tzanavaris P., Pihlström Y. M., Webb J. K., 2007, *MNRAS*, 382, 1331
- Curran S. J., Webb J. K., 2006, *MNRAS*, 371, 356
- Curran S. J., Webb J. K., Murphy M. T., Carswell R. F., 2004b, *MNRAS*, 351, L24
- Davis M. M., May L. S., 1978, *ApJ*, 219, 1
- Delhaize J., Meyer M. J., Staveley-Smith L., Boyle B. J., 2013, *MNRAS*, 433, 1398
- Ellison S., Kanekar N., and Prochaska J. X., Momjian E., Worseck G., 2012, *MNRAS*, 424, 293
- Feigelson E. D., Nelson P. I., 1985, *ApJ*, 293, 192
- Ferguson H. C. et al., 2004, *ApJ*, 600, L107
- Field G. B., 1959, *ApJ*, 129, 536
- Gupta N., Srianand R., Petitjean P., Noterdaeme P., Saikia D. J., 2009a, in *Astronomical Society of the Pacific Conference Series*, Vol. 407, *The Low-Frequency Radio Universe*, Saikia D. J., Green D. A., Gupta Y., Venturi T., eds., p. 67
- Gupta N., Srianand R., Petitjean P., Noterdaeme P., Saikia D. J., 2009b, *MNRAS*, 398, 201
- Hopkins A. M., Beacom J. F., 2006, *ApJ*, 651, 142
- Hoppmann L., Staveley-Smith L., Freudling W., Zwaan M. A., Minchin R. F., Calabretta M. R., 2015, *MNRAS*, 452, 3726
- Isobe T., Feigelson E., Nelson P., 1986, *ApJ*, 306, 490
- Kanekar N., 2014, *ApJ*, 797, L20
- Kanekar N., Chengalur J. N., 2001, *A&A*, 369, 42
- Kanekar N., Chengalur J. N., 2003, *A&A*, 399, 857
- Kanekar N., Chengalur J. N., Subrahmanyan R., Petitjean P., 2001a, *A&A*, 367, 46
- Kanekar N., Ellison S. L., Momjian E., York B. A., Pettini M., 2013, *MNRAS*, 532
- Kanekar N., Ghosh T., Chengalur J. N., 2001b, *A&A*, 373, 394
- Kanekar N., Lane W. M., Momjian E., Briggs F. H., Chengalur J. N., 2009a, *MNRAS*, 394, L61
- Kanekar N., Prochaska J. X., Ellison S. L., Chengalur J. N., 2009b, *MNRAS*, 396, 385
- Kanekar N. et al., 2014, *MNRAS*, 438, 2131
- Kanekar N., Smette A., Briggs F. H., Chengalur J. N., 2009c, *ApJ*, 705, L40
- Khare P., Kulkarni V. P., Péroux C., York D. G., Lauroesch J. T., Meiring J. D., 2007, *A&A*, 464, 487
- Lagos C. D. P., Baugh C. M., Zwaan M. A., Lacey C. G., Gonzalez-Perez V., Power C., Swinbank A. M., van Kampen E., 2014, *MNRAS*, 440, 920
- Lah P. et al., 2007, *MNRAS*, 376, 1357
- Lanfranchi G. A., Friaça A. C. S., 2003, *MNRAS*, 343, 481
- Lavalley M. P., Isobe T., Feigelson E. D., 1992, in *BAAS*, Vol. 24, pp. 839–840
- Ledoux C., Petitjean P., Fynbo J. U., Møller, P. and Srianand R., 2006, *A&A*, 457, 71
- Madau P., Dickinson M., 2014, *Ann. Rev. Astr. Ap.*, 52, 415
- Maiolino R. et al., 2005, *A&A*, 440, L51
- Murphy M. T., Curran S. J., Webb J. K., Ménager H., Zych B. J., 2007, *MNRAS*, 376, 673
- Neeleman M., Kanekar N., Prochaska J. X., Rafelski M., Carilli C. L., Wolfe A. M., 2017, *Science*, 355, 1285
- Neeleman M., Prochaska J. X., Ribaud J., Lehner N., Howk J. C., Rafelski M., Kanekar N., 2016, *ApJ*, 818, 113
- Noterdaeme P. et al., 2012, *A&A*, 547, L1
- O’Dea C. P., Baum S. A., Gallimore J. F., 1994, *ApJ*, 436, 669
- Peacock J. A., 1999, *Cosmological Physics*. Cambridge University Press, Cambridge
- Prochaska J. X., Chen H.-W., Wolfe A. M., Dessauges-Zavadsky M., Bloom J. S., 2008, *ApJ*, 672, 59
- Prochaska J. X., Gawiser E., Wolfe A. M., Castro S., Djorgovski S. G., 2003, *ApJ*, 595, L9
- Prochaska J. X., Herbert-Fort S., 2004, *PASP*, 116, 622
- Prochaska J. X., Herbert-Fort S., Wolfe A. M., 2005, *ApJ*, 635, 123
- Prochaska J. X., Wolfe A. M., 2009, *ApJ*, 696, 1543
- Purcell E. M., Field G. B., 1956, *ApJ*, 124, 542
- Rafelski M., Wolfe A. M., Prochaska J. X., Neeleman M., Mendez A. J., 2012, *ApJ*, 755, 89
- Rao S., Turnshek D., Nestor D. B., 2006, *ApJ*, 636, 610
- Rao S. M., Turnshek D. A., 2000, *ApJS*, 130, 1
- Rhee J., Zwaan M. A., Briggs F. H., Chengalur J. N., Lah P., Oosterloo T., van der Hulst T., 2013, *MNRAS*, 435, 2693
- Rohlfs K., Wilson T. L., 2000, *Tools of Radio Astronomy*. Springer-Verlag, Berlin
- Roy N., Mathur S., Gajjar V., Nath Patra N., 2013, *MNRAS*, 436, L94
- Sobral D., Smail I., Best P. N., Geach J. E., Matsuda Y., Stott J. P., Cirasuolo M., Kurk J., 2013, *MNRAS*, 428, 1128
- Srianand R., Gupta N., Petitjean P., Noterdaeme P., Ledoux C., Salter C. J., Saikia D. J., 2012, *MNRAS*, 421
- Trujillo I. et al., 2006, *ApJ*, 650, 18
- Tzanavaris P., Webb J. K., Murphy M. T., Flambaum V. V., Curran S. J., 2005, *PhRvL*, 95, 041301
- Wolfe A. M., Gawiser E., Prochaska J. X., 2003, *ApJ*, 593, 235
- Wolfe A. M., Prochaska J. X., 1998, *ApJ*, 494, L15
- Wolfire M. G., Hollenbach D., McKee C. F., Tielens A. G. G. M., Bakes E. L. O., 1995, *ApJ*, 443, 152
- York B. A., Kanekar N., Ellison S. L., Pettini M., 2007, *MNRAS*, 382, L53
- Zwaan M. A., van der Hulst J. M., Briggs F. H., Verheijen M. A. W., Ryan-Weber E. V., 2005, *MNRAS*, 364, 1467
- Zwart J. T. L., Jarvis M. J., Deane R. P., Bonfield D. G., Knowles K., Madhanpall N., Rahmani H., Smith D. J. B., 2014, *MNRAS*, 439, 1459